Hydrology Research

Hydrology Research Vol 55 No 2, 221 doi: 10.2166/nh.2024.144

Effect of mountainous rainfall on uncertainty in flood model parameter estimation

Jeonghoon Lee[a], Jeonghyeon Choi[b], Suhyung Jang[c] and Sangdan Kim[a,*]

[a] Division of Earth Environmental System Science (Major of Environmental Engineering), Pukyong National University, Busan 48513, Korea
[b] Hydro Science and Engineering Research Institute, Korea Institute of Civil Engineering and Building Technology (KICT), Goyangsi 10223 Korea
[c] Water Resources & Environmental Research Center, K-Water Research Institute, Daejeon 34350, Korea
*Corresponding author. E-mail: skim@pknu.ac.kr

SK, 0000-0001-6244-6612

ABSTRACT

Explaining the significant variability of rainfall in orographically complex mountainous regions remains a challenging task even for modern raingauge networks. To address this issue, a real-time spatial rainfall field estimation model, called WREPN (WRF Rainfall-Elevation Parameterized Nowcasting), has been developed, incorporating the influence of mountain effect based on ground raingauge networks. In this study, we examined the effect of mountainous rainfall estimates on the uncertainty of flood model parameter estimation. As a comparison, an inverse distance weighting technique was applied to ground raingauge data to estimate the spatial rainfall field. To convert the spatial rainfall fields into flood volumes, we employed the ModClark model, a conceptual rainfall–runoff model with distributed rainfall input. Bayesian theory was applied for parameter estimation to incorporate uncertainty analysis. The ModClark model demonstrated good flood reproducibility regardless of the estimation method for spatial rainfall fields. Parameter estimation results indicated that the WREPN spatial rainfall field, which accounted for the influence of the mountain effect, led to lower curve numbers due to higher estimated rainfall compared to the IDW spatial rainfall field, while the concentration time and storage coefficient showed minimal differences.

Key words: Modclark model, mountainous watershed, orographic rainfall, spatial rainfall field, uncertainty analysis

HIGHLIGHTS

- The study introduces the WREPN model, which incorporates the influence of mountain effect in rainfall estimation, leading to reduced uncertainty in flood model parameter estimation compared to traditional methods like IDW.
- Utilizing the ModClark model for converting spatial rainfall fields into flood volumes, the study demonstrates good flood reproducibility regardless of the spatial rainfall field estimation method used.
- By applying Bayesian theory for parameter estimation, the study shows that the WREPN spatial rainfall field results in lower curve numbers and more accurate flood estimations compared to the IDW spatial rainfall field, highlighting the importance of considering mountainous rainfall effects in hydrological modeling.

GRAPHICAL ABSTRACT

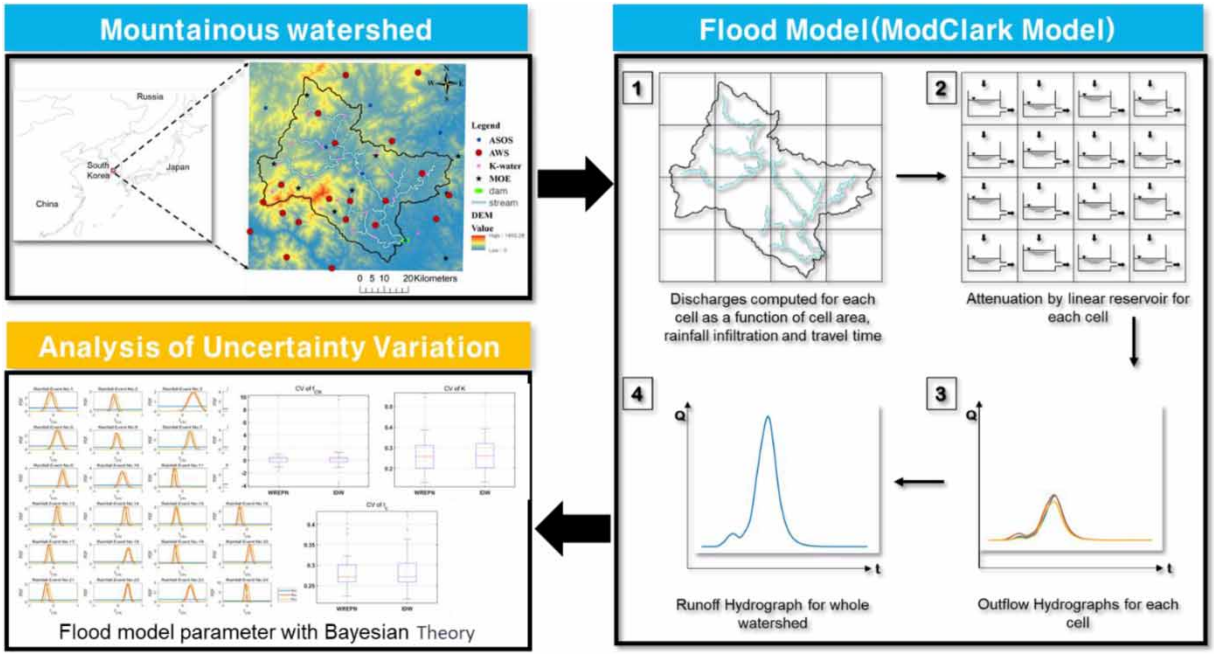

1. INTRODUCTION

Flooding is one of the most common natural disasters on Earth, and flooding events caused by extreme rainfall are increasing worldwide today, anticipated to occur more frequently as a consequence of the changing climate (Mie Sein *et al.* 2021; Hailemariam & Alfredsen 2023; Kirsta & Troshkova 2023). The Korean Peninsula has recently experienced frequent occurrences of heavy rainfall and extreme weather conditions close to super typhoons, resulting in significant damages (Lee & Choi 2018). Numerous studies on flood risk prediction indicate an increasing likelihood of future flooding events, with climate change scenarios suggesting a potential rise in both the frequency and magnitude of flood events in many regions (Kundzewicz *et al.* 2019; Klijn *et al.* 2022).

Rainfall is one of the most critical factors influencing flooding. The amount and patterns of rainfall can vary significantly from one region to another, influenced by geographical, climatic, and topographical factors (Houze 2012; Furcolo *et al.* 2016). Rainfall plays a crucial role as an input for hydrological modeling. However, its distribution across the watershed is often non-uniform, resulting in significant uncertainties in estimated model parameters when the detailed spatial variation of input rainfall is not considered (Obled *et al.* 1994; Zhang & Han 2017). Consequently, the spatial characteristics of rainfall directly affect the results of local flood simulations, determining the scale and impacts of flood damages (Singh 1997; Arnaud *et al.* 2002; Gabellani *et al.* 2007; Younger *et al.* 2009; Emmanuel *et al.* 2015). One of the main sources of rainfall increase in mountainous watersheds is the orographic effect, also known as the mountain effect, resulting from atmospheric uplift by hills and mountains (Barry 1992; Abbate *et al.* 2022; Auliagisni *et al.* 2022). The interaction between atmospheric circulation and relief results, among other effects, in increasing rainfall with elevation (Lloyd 2005; Tobin *et al.* 2011; Gottardi *et al.* 2012). Consequently, rainfall in mountainous regions may not be adequately captured by conventional raingauge networks due to the topographical characteristics, which may negatively affect the accuracy of flood estimation. The accurate estimation of the spatial distribution of rainfall requires a very dense network of instruments, which entails large installation and operational costs (Goovaerts 2000). As a result, rainfall estimation in mountainous regions, particularly in ungauged areas and high elevation catchments, remains a true challenge for hydrological modeling (Piman & Babel 2013; Skaugen *et al.* 2015; Hussain *et al.* 2018). This challenge is mainly due to the high spatial variability and scarcity of observations in those areas (Krajewski *et al.* 2000; Gottardi *et al.* 2012; Stoffel *et al.* 2016; Ragettli *et al.* 2021).

In cases where the density of raingauge networks is too low to provide sufficient data, estimations are often generated based on data recorded at nearby gauges. However, in such cases, significant discrepancies can arise (Xiaojun *et al.* 2021). For

instance, in the Namgang Dam area in Korea, there has been a recorded rainfall–runoff ratio exceeding 1 (Lee *et al.* 2023). Similarly, in Zhouqu, China, a raingauge located 16 km from headwaters recorded 96 mm of rainfall, while only 3 mm was recorded at the outlet raingauge (Hu *et al.* 2010; Cui *et al.* 2013). Xiaojun *et al.* (2021) analyzed the empirical relationship between rainfall and both the elevation and the density of rain gauges based on 52 storm events that occurred in mountainous watersheds. Their study demonstrated that estimating rainfall distribution at high elevations is more challenging, and they analyzed the uncertainty caused by raingauge selection in hydrological hazards forecasting. According to the error analysis, uncertainties increased when the horizontal distance between gauges exceeded 3 km. Such results exemplify the scale of the variation and uncertainty associated with rainfall in mountainous watersheds.

Therefore, recent studies on estimating rainfall in mountainous watersheds, referred to as mountainous rainfall, or flood estimation have been continuously conducted using radar or satellite rainfall data. Gebregiorgis & Hossain (2012) demonstrated that the uncertainty of satellite rainfall data depends more on the topography than on the regional climate. Moreno *et al.* (2014) aimed to simulate flow rates based on radar rainfall and address the uncertainties associated with rainfall estimation from radar data. Nikolopoulos *et al.* (2014) sought to define the impact of uncertainties related to mountainous rainfall estimation based on ground raingauge and predict the occurrence probability of debris flows. Adib *et al.* (2019) performed uncertainty and sensitivity analysis to find the optimal rainfall–runoff model for flood estimation in mountainous watersheds. Saouabe *et al.* (2020) evaluated the accuracy of satellite rainfall data and its suitability for hydrological modeling in mountainous watersheds, confirming its applicability in ungauged or data-scarce regions. However, these studies mainly focus on the suitability assessment, uncertainties of mountainous rainfall or flood volume, and research regarding the uncertainty of flood estimation associated with mountainous rainfall remains limited.

In this study, we examine the effect of the estimated spatial rainfall field on the uncertainty of flood estimation by comparing two methods: the WREPN (WRF Rainfall-Elevation Parameterized Nowcasting) model and the IDW (Inverse Distance Weighting) method. The WREPN model is developed to estimate the real-time spatial rainfall field considering the mountain effect based on ground raingauge data, while the IDW method is widely used in practice.

2. DATA AND METHODS

2.1. Study area

The Namgang Dam watershed is a representative mountainous region in the Korea, with a highest elevation of 1,853 m and a lowest elevation of 35 m based on a digital elevation model with a spatial resolution of 90 m. The Namgang Dam watershed is characterized by steep mountainous terrain with flat-gradient river networks, particularly in the lower reaches. The watershed has a mean slope of 12% with a maximum of 45%. The channel network has a mean width of 25 m with a maximum of 805 m near the reservoir (Vieux *et al.* 2009). As Figure 1 indicates, there are 55 ground raingauges operational in this watershed.

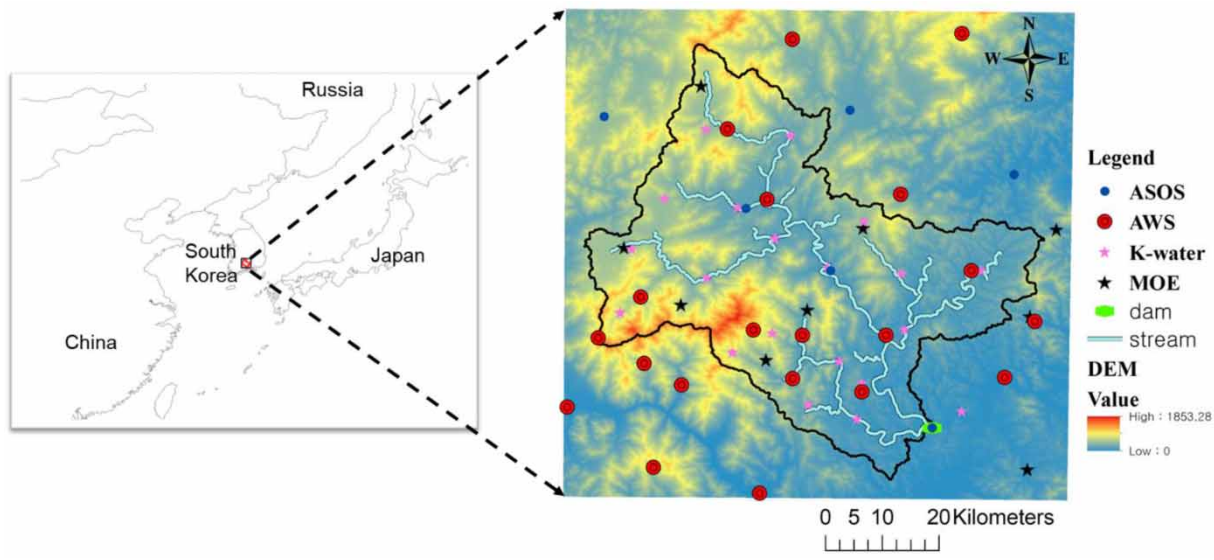

Figure 1 | Study area and the ground observation station.

Raingauges are classified into four categories depending on the operating agency. They are the ASOS (Automated Synoptic Observing System) and AWS (Automatic Weather System) operated by the Korea Meteorological Administration, the observation networks of K-water (formerly Korea Water Resources Corporation), and the MOE (Korea Ministry of Environment) observation network. Among these gauges, the one at the lowest elevation is situated at EL 4.5 m, while the one at the highest elevation is positioned at 1,087.9 m (Lee *et al.* 2023). The watershed receives an annual-mean rainfall of 1,584.2 mm, about 1.2 times of the annual-mean rainfall in Korea (1,274 mm), most of it in summer and early fall (June–September) when the region is affected by the East Asia monsoon, tropical cyclones and thunderstorms (Ryu *et al.* 2021).

2.2. Target storm events

The selection of target storm events in the Namgang Dam watershed was carried out by analyzing the time series data from the ground raingauge. To separate the storm events, the Inter-Event Time Definition (IETD) method (Kim & Han 2010; Joo *et al.* 2013) was applied with a threshold of 12 h. This approach led to the identification of 24 individual storm events characterized by high rainfall depth. Subsequent analyses were then performed for these 24 events, as summarized in Table 1.

The spatial rainfall fields for the target storm events were estimated using two methods: the WREPN model (Lee *et al.* 2023) and the IDW technique. Both rainfall fields have a spatial resolution of 3 km. The WREPN model is a parameterized model that takes into account the mountain effect on rainfall estimation. It incorporates the Weather Research and Forecasting (WRF) model, which is a regional-scale climate model, to establish the relationship between hourly rainfall and elevation at a regional scale. By utilizing the hourly rainfall data from the ground raingauge network, the WREPN model can provide real-time spatial rainfall field estimates. For a more comprehensive understanding, please refer to the study by Lee *et al.* (2023).

Table 1 | Target storm events in this study

Event no.	The time the storm event occurred	Duration (h)	Rainfall depth (mm)	Antecedent 5-day rainfall (mm)
1	2020. 08. 05. 07:00	93	380.30	11.14
2	2012. 08. 21 08:00	97	259.66	11.16
3	2012. 09. 16. 01:00	39	252.34	5.41
4	2018. 08. 25. 14:00	62	242.36	105.41
5	2018. 10. 04. 22:00	38	227.09	1.00
6	2014. 08. 01. 22:00	76	219.35	8.08
7	2020. 07. 12. 11:00	80	188.07	75.60
8	2013. 07. 04. 02:00	49	182.90	37.82
9	2014. 08. 17. 17:00	89	168.52	31.49
10	2015. 07. 11. 14:00	49	157.08	90.66
11	2016. 07. 01. 10:00	80	136.12	0.99
12	2012. 08. 27. 20:00	27	121.52	224.65
13	2012. 07. 13. 01:00	66	115.31	84.06
14	2018. 06. 29. 21:00	103	109.08	134.09
15	2014. 09. 23. 20:00	26	104.87	0.21
16	2013. 08. 21. 19:00	80	102.08	6.23
17	2013. 05. 27. 12:00	32	98.62	0.72
18	2018. 09. 02. 14:00	42	90.31	46.39
19	2015. 07. 07. 11:00	48	84.65	0.17
20	2012. 04. 21. 05:00	23	79.75	6.68
21	2018. 08. 23. 01:00	39	76.29	0.37
22	2012. 09. 07. 20:00	12	74.96	21.85
23	2016. 10. 05. 00:00	14	72.73	31.87
24	2017. 08. 19. 13:00	86	69.40	36.45

2.3. Modclark model

In this study, the flood estimation was conducted using the ModClark model, which is based on the fundamental principles of Clark's conceptual rainfall–runoff model (Clark 1945). The ModClark model is an enhanced version with the addition of a spatially distributed rainfall input feature (Figure 2). Its capability for rainfall–runoff analysis using spatial rainfall fields has been demonstrated in various regions and climates through several previous studies (Yoon *et al.* 2002; Paudel *et al.* 2009; Cho *et al.* 2018; Lee & Yoo 2023).

In the ModClark model, the accumulated excess rainfall from each grid cell is routed through a linear reservoir. The model's parameters consist of three elements: the curve number (CN) for effective rainfall estimation, the time of concentration (t_c), and the storage coefficient (K). As the antecedent soil moisture conditions vary for each heavy rainfall event, the CN values are estimated separately for each storm event.

The ModClark model's ability to incorporate spatially distributed rainfall input makes it suitable for analyzing flood events in different geographical areas, providing a valuable tool for flood estimation in mountainous regions where rainfall distribution can be highly variable.

The performance evaluation of the ModClark model was conducted using four metrics. The coefficient of determination (R^2) is defined as the ratio of the covariance and standard deviations between observed and simulated values, and it can be calculated using the following equation.

$$R^2 = \left[\frac{\sum_{i=1}^{n} (Q_o - \overline{Q_o})(Q_s - \overline{Q_s})}{\sqrt{\sum_{i=1}^{n} (Q_o - \overline{Q_o})^2} \sqrt{\sum_{i=1}^{n} (Q_s - \overline{Q_s})^2}} \right]^2 \quad (1)$$

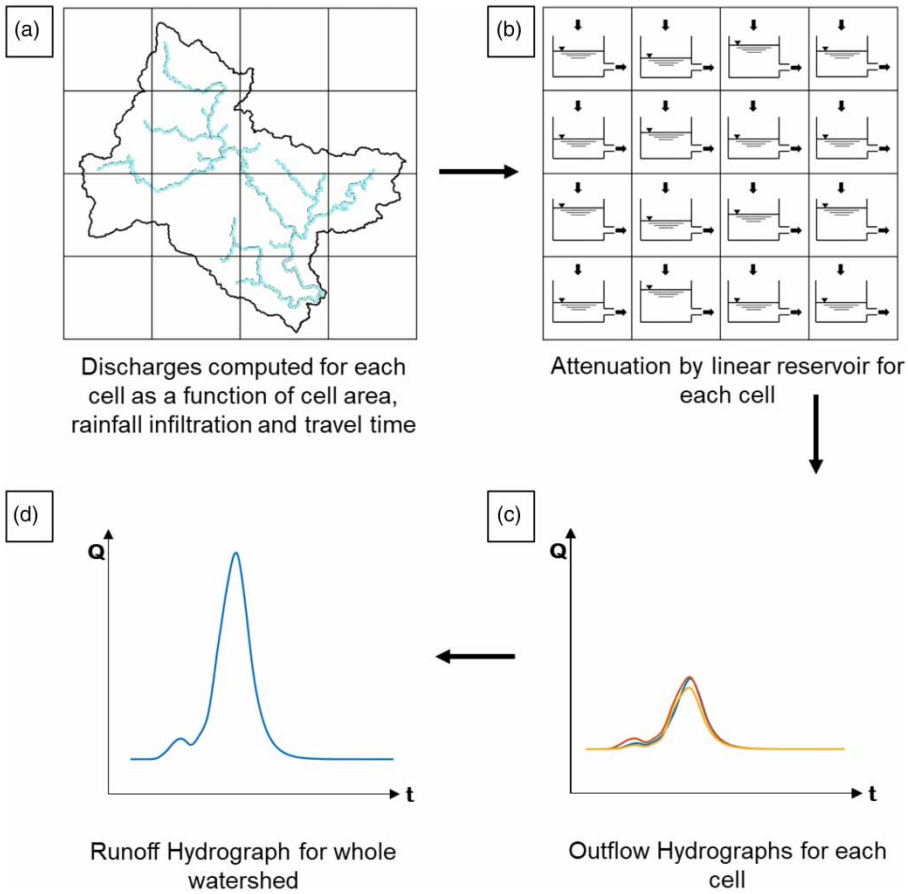

Figure 2 | Conceptual diagram of the Modclark model.

The Nash–Sutcliffe efficiency (NSE) is a metric used to evaluate the efficiency of a model by comparing the relative size between the variance of the residuals and the variance of the observations, and can be calculated using the following equation.

$$\mathrm{NSE} = 1 - \frac{\sum_{i=1}^{n} (Q_o - Q_s)^2}{\sum_{i=1}^{n} (Q_o - \overline{Q_o})^2} \tag{2}$$

The Kling–Gupta efficiency (KGE) is a metric developed to address the shortcomings of NSE by considering the variance, correlation coefficient, and mean simultaneously. It can be calculated using the following equation.

$$\mathrm{KGE} = 1 - \sqrt{(\gamma - 1)^2 + (\alpha - 1)^2 + (\beta - 1)^2} \tag{3}$$

In the equations mentioned above, γ represents the linear correlation coefficient between the observed and simulated values, α represents the ratio of the standard deviation of the simulated values to the standard deviation of the observed values, and β represents the ratio of the mean of the simulated values to the mean of the observed values. For all three metrics, R^2, NSE, and KGE, values closer to 1 indicate better model performance, meaning that the model's simulated results are closer to the observed values.

PBIAS (Percent Bias) evaluates whether the model's results are generally underestimating or overestimating the observed values. It is calculated using Equation (4). When PBIAS is positive, it indicates that the simulated results are underestimated, and when it is negative, it means the simulated results are overestimated. Therefore, PBIAS is considered to have better model performance when its absolute value is closer to zero.

$$\mathrm{PBIAS} = \frac{\sum_{i=1}^{n} (Q_o - Q_s)}{\sum_{i=1}^{n} Q_o} \times 100 \tag{4}$$

2.3.1. Watershed and stream network

In this study, the stream network of the watershed was established by upscaling the digital elevation model with a spatial resolution of 90 m to match the spatial rainfall field with a spatial resolution of 3 km. To achieve this implementation, the D-8 algorithm proposed by O'Callaghan & Mark (1984) was applied.

The watershed was divided into square grid cells, and the travel time for each grid cell to reach the watershed outlet was calculated using Equation (5). This equation is based on the number of cells traversed by each grid cell to reach the watershed outlet and the maximum number of cells traveled in the longest distance.

$$(\text{Travel time})_{\text{cell}} = t_c \frac{(\text{Travel length})_{\text{cell}}}{\text{Max(Travel length)}} \tag{5}$$

The grid cell's travel time and contributing area relationship are determined based on the following equation, which is referenced from the HEC-HMS Technical Reference Manual (Feldman 2000):

$$\frac{A_t}{A} = \begin{cases} 1.414\left(\dfrac{t}{t_c}\right)^{1.5} & \text{for } t \le \dfrac{t_c}{2} \\ 1 - 1.414\left(1 - \dfrac{t}{t_c}\right)^{1.5} & \text{for } t \ge \dfrac{t_c}{2} \end{cases} \tag{6}$$

In this context, A_t represents the contributing area at time t, which is the area that contributes to the flow at a specific time in the watershed. A refers to the total watershed area, which is the entire area of the watershed under consideration.

The routing coefficient C is determined using the storage coefficient K and is calculated as the following equation

$$C = \frac{2\Delta t}{2K + \Delta t} \tag{7}$$

where Δt represents the computation time interval.

To derive the instantaneous unit hydrograph using the routing coefficient and the travel time-area relationship, the following equation is used:

$$\mathrm{IUH}_t = \frac{1}{2}C(\mathrm{TA}_t + \mathrm{TA}_{t-1}) + (1 - C)\mathrm{IUH}_{t-1} \tag{8}$$

The final synthetic unit hydrograph is obtained by averaging the instantaneous unit hydrographs as shown in the following equation.

$$\mathrm{UH} = \frac{1}{2}(\mathrm{IUH}_t + \mathrm{IUH}_{t-1}) \tag{9}$$

2.3.2. NRCS-CN method

In the ModClark model, the NRCS-CN method (USDA 1986) was applied to calculate the rainfall–runoff process. The runoff Q for a given storm event is computed using Equation (10) as follows:

$$Q = \frac{(P - I_a)^2}{P - I_a + S}, \ P \geq I_a \tag{10}$$

P represents the rainfall amount, and the initial abstraction I_a is assumed to be 0.2. The calculation of the maximum potential retention capacity (S) is based on the following equation:

$$S = \frac{25,400}{\mathrm{CN}} - 254 \tag{11}$$

The initial Curve Number (CN_o) values are generated on a grid cell basis using information on land use and soil type provided by the Korean Water resources Management Information System (WAMIS) at http://wamis.go.kr/. The final CN value (i.e., CN_i) for cell i is determined as shown in Equation (12) below by applying a correction factor, denoted as f_{CN}.

$$\mathrm{CN}_i = CN_{o,i} + f_{\mathrm{CN}}(100 - \mathrm{CN}_{o,i}) \tag{12}$$

In this context, $\mathrm{CN}_{o,i}$ represents the initial CN value for cell i. The correction factor f_{CN} is considered to be a single value applied uniformly across the entire watershed

2.4. Parameter estimation

The parameters of ModClark model are estimated using Bayesian theory account for uncertainty analysis, and the posterior distribution of the parameters is given by the following equation:

$$\pi(\theta|Q) = \frac{\pi(Q|\theta)\pi(\theta)}{\pi(Q)} \tag{13}$$

where $\pi(\theta|Q)$ is the posterior distribution of the parameters θ given the observed flow data(Q), $\pi(Q|\theta)$ is the likelihood of the observed flow data given the parameters θ, $\pi(\theta)$ is the prior distribution representing our prior belief or knowledge about the parameters before observing the data, $\pi(Q)$ is the marginal likelihood, which acts as a normalization constant to ensure that the posterior distribution is a valid probability distribution.

In this study, the likelihood function is defined based on the assumption that the model errors are independent and normally distributed. It is represented by the following equation:

$$\pi(Q|\theta) = \prod_{i=1}^{n} \frac{1}{\sigma\sqrt{2pi}} e^{-\frac{1}{2}\left(\frac{Q_{o,i} - Q_{s,i}}{\sigma}\right)^2} \tag{14}$$

where $Q_{o,i}$ is the observed flow data at time step i, $Q_{s,i}$ is the corresponding model output (simulation) at time step i using the parameters θ, σ is the standard deviation of observed flow data.

The Metropolis–Hastings (hereafter MH) algorithm (Hastings 1970) was employed as the sampling algorithm to extract samples from the posterior distribution. The MH algorithm, as a general form of Markov Chain Monte Carlo (MCMC), is an attractive choice for generating samples from the posterior distribution and has proven successful in numerous cases (Wu *et al.* 2019; Liu *et al.* 2021).

3. RESULTS

3.1. Modclark model performance evaluation

Table 2 presents the results of the four performance evaluation metrics for the ModClark model. Both the WREPN and IDW spatial rainfall fields show excellent performance, with an average R^2 of 0.90, NSE of 0.88, and KGE of 0.83. Based on these results, it can be concluded that the ModClark model performs well, and no significant issues were identified regarding the estimation methods for spatial rainfall fields. Overall, the model successfully reproduces the flood timeseries, indicating its robustness and accuracy.

3.2. Parameter estimation results

The observed streamflow used for parameter estimation was obtained after baseflow separation from the inflow data of the Namgang Dam. Baseflow separation was conducted using a graphical method. Although various methods for baseflow separation exist, it was found that the choice of method had minimal effect on parameter estimation and overall results. Therefore, the details of the baseflow separation method were excluded.

The estimated parameters for each target storm event using different spatial rainfall estimation methods are shown in Table 3. It can be observed that all three parameters vary for each storm event. Comparing with the IDW spatial rainfall, the WREPN spatial rainfall consistently resulted in lower values of f_{CN}. For the 12th storm event, the highest CN value was estimated, which is attributed to the influence based on the antecedent 5-day rainfall that resulted in 224.65 mm (refer to Table 1 for details).

The concentration time (t_c) was consistently estimated to be an average of 14.75 h for both spatial rainfall estimation methods. However, there were two storm events (Nos 11, 19) with t_c values exceeding 20 h. This can be attributed to the relatively dry antecedent conditions of the watershed, where the antecedent 5-day rainfall for events 11 and 19 was only 0.99 and 0.17 mm, respectively.

Regarding the storage constant (K), there was no significant difference between WREPN (average 7.15) and IDW (average 7.21). However, the ninth storm event had the highest K value, estimated at 10.6. The considerable variation in these three parameters for different storm events is likely influenced by the antecedent rainfall conditions and other factors affecting the watershed's state during each event.

Figure 3 shows the posterior distributions of the parameter f_{CN} for each storm event. The posterior distributions of t_c and K did not exhibit significant differences, so they are included in Supplementary material (Figure S2). Comparing the two spatial rainfall estimation methods, WREPN's f_{CN} posterior distribution is shifted to the left compared to IDW's distribution. This observation can be attributed to the fact that WREPN considers mountain effects in the rainfall estimation process. Consequently, WREPN tends to estimate higher rainfall amounts compared to IDW, resulting in lower f_{CN} values.

3.3. Uncertainty analysis by parameter

Table 4 presents the coefficient of variation (CV) for the parameters based on different spatial rainfall estimation methods. Among the three parameters, f_{CN} exhibited a noticeably lower mean CV when estimated using the WREPN spatial rainfall. However, for t_c and K, there were no significant differences in the CV between the two methods. This can be attributed to the

Table 2 | ModClark model performance evaluation by the spatial rainfall field estimation method

	R^2		NSE		KGE		PBIAS (%)	
Event no.	WREPN	IDW	WREPN	IDW	WREPN	IDW	WREPN	IDW
1	0.9068	0.9094	0.8928	0.8966	0.7801	0.7912	−19.246	−17.743
2	0.9439	0.9497	0.9408	0.9458	0.9095	0.9030	−7.701	−8.650
3	0.8954	0.8997	0.8409	0.8430	0.6979	0.6985	−9.763	−8.451
4	0.9075	0.9156	0.9047	0.9140	0.9432	0.9497	−3.100	−2.390
5	0.9272	0.9293	0.9059	0.9086	0.7664	0.7697	−17.704	−17.574
6	0.9532	0.9550	0.9464	0.9499	0.8608	0.8794	−12.911	−10.716
7	0.9603	0.9620	0.9379	0.9409	0.7555	0.7695	−21.097	−19.306
8	0.9549	0.9546	0.9465	0.9459	0.8683	0.8672	−8.907	−8.689
9	0.7024	0.7195	0.6620	0.6810	0.6432	0.6543	−24.892	−24.023
10	0.9731	0.9750	0.9671	0.9692	0.8922	0.8977	−8.168	−7.018
11	0.8616	0.8683	0.8576	0.8655	0.9275	0.9300	−0.465	−0.572
12	0.8961	0.8974	0.8782	0.8782	0.7943	0.7933	−10.680	−9.333
13	0.9079	0.9089	0.8858	0.8891	0.8696	0.8749	10.619	10.518
14	0.8716	0.8811	0.8709	0.8794	0.9135	0.9187	−2.222	−3.656
15	0.9367	0.9348	0.9281	0.9259	0.8662	0.8606	−7.257	−9.823
16	0.9185	0.9209	0.9184	0.9205	0.9340	0.9383	−1.029	−2.797
17	0.9718	0.9729	0.9654	0.9666	0.9027	0.9025	−4.391	−5.675
18	0.9277	0.9288	0.9140	0.9155	0.8165	0.8200	−11.874	−11.477
19	0.9026	0.9000	0.8986	0.8952	0.8774	0.8696	−5.449	−4.069
20	0.9713	0.9718	0.9517	0.9512	0.8437	0.8404	−6.362	−6.434
21	0.8678	0.8681	0.8449	0.8452	0.7424	0.7419	−17.441	−17.672
22	0.8042	0.8010	0.7925	0.7862	0.7659	0.7504	−3.718	−1.722
23	0.7575	0.7618	0.7170	0.7243	0.6441	0.6545	−8.604	−8.238
24	0.8371	0.8373	0.8335	0.8345	0.8783	0.8810	6.016	5.264
Mean	0.8982	0.9010	0.8834	0.8863	0.8289	0.8315	−8.181	−7.927

fact that WREPN's rainfall data effectively captures the mountainous rainfall effect, leading to reduced uncertainty in the most rainfall-sensitive parameter, f_{CN}. Particularly, significant differences in the CV were observed for rainfall events 1 and 6. However, no strong association between antecedent rainfall amounts or rainfall amount of storm events and the CV was evident for other cases.

4. DISCUSSION

4.1. ModClark model performance evaluation

The performance evaluation of the ModClark model has shown favorable results overall, but some limitations have been observed in Table 2. In the case of PBIAS, the WREPN spatial rainfall field shows an average of −8.18%, and the IDW spatial rainfall field shows an average of −7.93%, indicating that the flood discharge was generally overestimated. Additionally, upon examining Figure S1 (supplementary material), it can be observed that some peak flows were underestimated in certain rainfall events. Nevertheless, considering the main objective of this study, which is to investigate the uncertainty in flood discharge estimation based on different spatial rainfall field estimation methods, it is deemed feasible to proceed with the analysis. More detailed results for each rainfall event and the corresponding simulated time series can be visualized and further assessed in Figure S1.

Table 3 | Parameter estimation results by the spatial rainfall field estimation method

	IDW			WREPN		
Event no.	f_{CN}	t_c	K	f_{CN}	t_c	K
1	−0.039	8.089	5.106	−0.130	8.093	5.082
2	−0.084	10.519	6.008	−0.174	10.462	5.936
3	0.489	8.117	5.298	0.435	8.194	5.335
4	0.219	10.078	5.837	0.144	9.829	5.757
5	0.218	9.570	5.625	0.153	9.559	5.639
6	0.010	8.659	5.598	−0.057	8.581	5.460
7	0.381	10.451	5.938	0.303	10.251	5.891
8	0.175	11.912	6.225	0.109	11.658	6.221
9	0.446	14.441	10.656	0.368	14.027	10.619
10	0.257	10.520	6.131	0.174	10.474	6.097
11	−0.266	22.758	7.097	−0.349	22.825	7.083
12	0.493	11.238	6.294	0.438	11.024	6.208
13	0.224	14.920	9.877	0.144	14.533	9.672
14	0.390	18.782	9.211	0.285	18.200	8.853
15	−0.209	14.881	7.154	−0.270	15.052	6.953
16	−0.231	20.624	8.510	−0.318	20.180	8.531
17	−0.121	12.871	7.068	−0.188	12.846	7.044
18	0.465	12.657	6.729	0.416	12.617	6.845
19	−0.213	29.189	8.248	−0.302	29.643	8.184
20	0.176	17.747	8.120	0.099	17.829	8.098
21	−0.207	18.493	7.367	−0.305	18.176	7.330
22	0.435	17.486	7.235	0.396	17.511	7.190
23	0.363	18.147	7.729	0.314	18.066	8.175
24	0.034	21.930	10.071	−0.065	24.454	9.324
Mean	0.142	14.75	7.21	0.068	14.75	7.15

In Figure S1, we see particular underestimation in certain peak flows, especially the first peak. These limitations could be attributed to various factors.

Firstly, one of the limitations could be related to the application of the NRCS-CN method used to calculate the runoff from rainfall. As it was originally developed to estimate daily runoff, errors may arise when applied at an hourly or sub-hourly time resolution (Verma *et al.* 2017). Previous studies have highlighted significant uncertainties when applying the NRCS-CN method in complex forested areas with various soil, land cover, and terrain conditions (Tedela *et al.* 2012). In this study, the initial CN values were determined based on the CN-*II* condition, and the correction factor f_{CN} was estimated as a parameter, resulting in the final CN values. However, the process of determining the initial CN values did not consider factors such as antecedent soil moisture, vegetation effects, and terrain, leading to inherent uncertainties.

Secondly, the use of 3 km grid cells to construct the spatial rainfall field could lead to limitations. Local extreme rainfall events might not be captured by the gauge stations, or if captured, the process of estimating spatial average values during interpolation could lead to smoothing, potentially resulting in underestimation or overestimation of the input rainfall. According to Sangati & Borga (2009), an important error source related to spatial rainfall aggregation is the rainfall volume error caused by incorrectly smoothing the rainfall volume either inside or outside of the watershed. Previous studies have shown significant improvement in simulated streamflow dynamics and accuracy when using higher resolution (1 km) spatial rainfall fields (Lobligeois *et al.* 2014). Especially in mountainous regions with high rainfall variability and

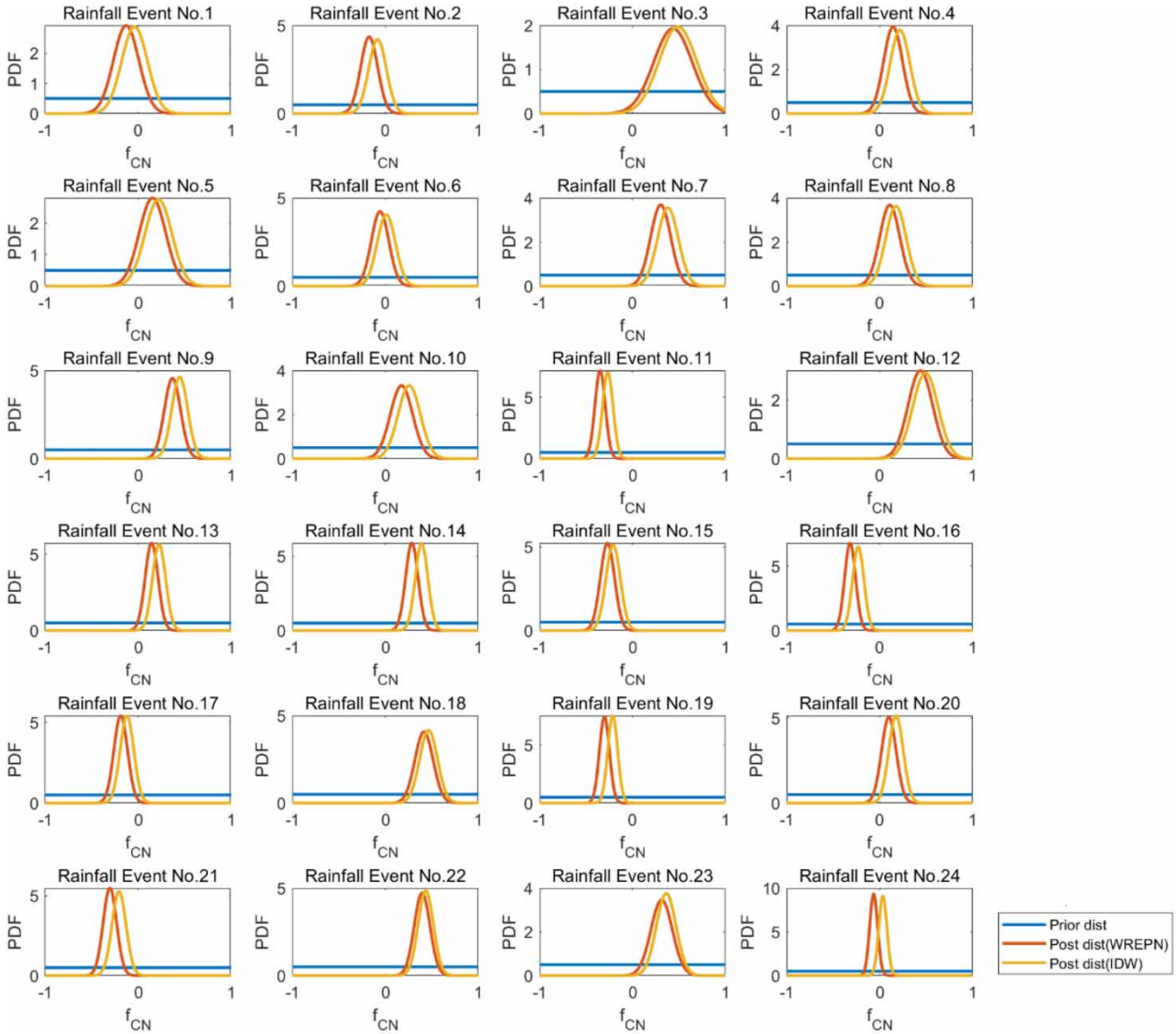

Figure 3 | Posterior distribution of the parameter f_{CN} for each spatial rainfall field estimation method.

low observation density, uncertainties are likely to be significant. Rainfall events 22 and 23 were particularly underestimated at the peak, and there is a possibility that the problem caused by the low resolution was intensified as the rainfall duration was short.

To address these issues, improvements in the spatial rainfall estimation method by incorporating high-resolution radar rainfall or weather model outputs could be considered. However, the high computational cost remains a challenge for flood forecasting applications.

4.2. Uncertainty of parameter

Through the assessment of parameter uncertainty, it was observed that the use of WREPN spatial rainfall field reduces the uncertainty in estimating flood model parameters, particularly in the variability of the parameter f_{CN}, compared to the IDW spatial rainfall field. This significant reduction in the CV of f_{CN} for events 1, 2, and 6 in WREPN could be attributed to the fact that these events exhibit much higher observed accumulated rainfall (654, 506.5, and 596.5 mm, respectively) compared to other events (Figure 4). Consequently, it can be hypothesized that the WREPN spatial rainfall field, which considers elevation effects, might be able to reduce the uncertainty in flood model parameter estimation for extreme events with

Table 4 | Coefficient of variation for the parameters based on different spatial rainfall estimation methods

	IDW			WREPN		
Event no.	f_{CN}	t_c	K	f_{CN}	t_c	K
1	3.5381	0.2267	0.1336	1.0537	0.2245	0.1310
2	1.1249	0.2808	0.1974	0.5252	0.2764	0.1954
3	0.4139	0.2232	0.1737	0.4747	0.2274	0.1752
4	0.4806	0.2706	0.2025	0.7040	0.2705	0.1975
5	0.6642	0.2712	0.2025	0.9282	0.2705	0.2049
6	9.5818	0.2624	0.1829	1.6506	0.2568	0.1696
7	0.2941	0.2817	0.2022	0.3565	0.2714	0.1980
8	0.6259	0.2953	0.2324	0.9979	0.2974	0.2397
9	0.1927	0.2822	0.2437	0.2372	0.2741	0.2338
10	0.4677	0.3154	0.2294	0.6916	0.3227	0.2246
11	0.2128	0.2176	0.2509	0.1596	0.2314	0.2544
12	0.2754	0.2710	0.2582	0.3023	0.2714	0.2569
13	0.3144	0.3594	0.2808	0.4816	0.3780	0.2824
14	0.1743	0.2806	0.2664	0.2366	0.2859	0.2580
15	0.3717	0.3179	0.2990	0.2823	0.3046	0.2818
16	0.2663	0.2724	0.3268	0.1852	0.2758	0.3154
17	0.6110	0.3880	0.2755	0.3910	0.3893	0.2742
18	0.2058	0.2477	0.2620	0.2350	0.2555	0.2727
19	0.2496	0.2635	0.3730	0.1787	0.2582	0.3871
20	0.4404	0.3642	0.3470	0.7976	0.3893	0.3445
21	0.3655	0.2557	0.3268	0.2377	0.2611	0.3077
22	0.1888	0.2563	0.3739	0.2129	0.2618	0.3568
23	0.2925	0.2646	0.3924	0.3673	0.2669	0.5453
24	1.2706	0.4210	0.3137	0.6588	0.4018	0.3161
Mean	0.9426	0.2871	0.2644	0.5144	0.2884	0.2676

exceptionally high rainfall amounts. However, to draw more generalized conclusions, further analysis on a larger number of events and the utilization of detailed spatial data such as radar rainfall are warranted. Additionally, it should be noted that the selection of target rainfall events in this study was based on total rainfall amount. Another approach to consider could be selecting target events based on observed flood discharge. Combining both approaches could provide valuable insights for future studies.

Finally, the box plots of the CV for each event are shown in Figure 5. It is evident that for all three parameters, IDW exhibits a wide range between the maximum and minimum CV. In contrast, the use of the WREPN spatial rainfall field results in consistent uncertainty across events, indicating lower overall uncertainty compared to IDW. This indirect evidence further supports the fact that the WREPN spatial rainfall field reduces the uncertainty in flood discharge estimation compared to IDW by exhibiting more consistent uncertainty across storm events.

5. CONCLUSIONS

In this study, we aimed to estimate floods using the WREPN model, which was developed to realistically estimate rainfall in mountainous areas that are difficult to capture with ground raingauge networks. We compared the flood estimations using the WREPN-based spatial rainfall field with the commonly used IDW-based spatial rainfall field to examine the effect of spatial rainfall estimation on the uncertainty of flood model parameter estimation. For the hydrological analysis of the spatial rainfall

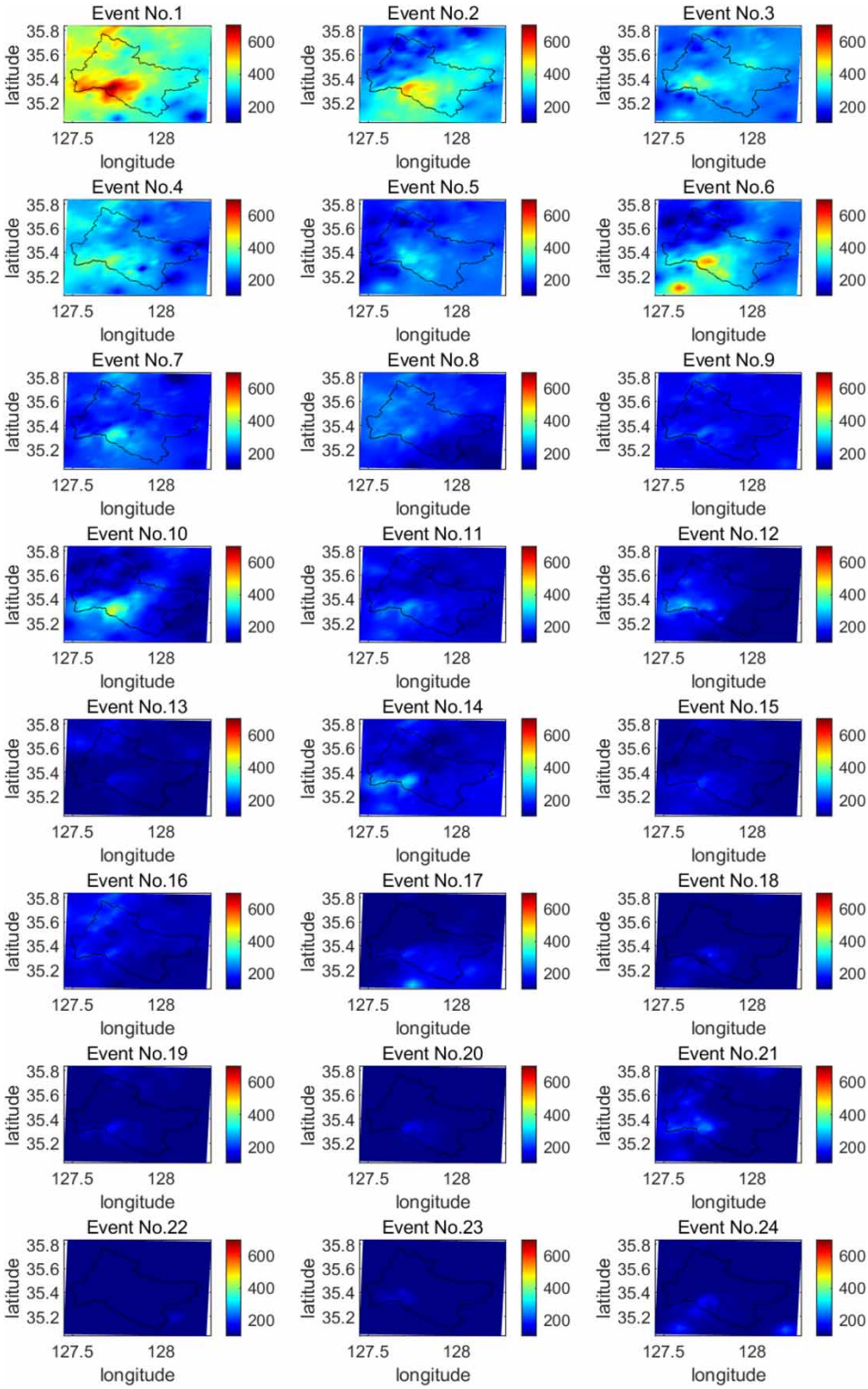

Figure 4 | Accumulated rainfall field by target storm event.

fields, we utilized the ModClark model, which operates on a grid-based approach and demonstrated its capability to accurately reproduce observed flood discharge through performance evaluation. To assess the uncertainty in flood model parameter estimations, we employed Bayesian techniques for parameter estimation in the ModClark model. The results

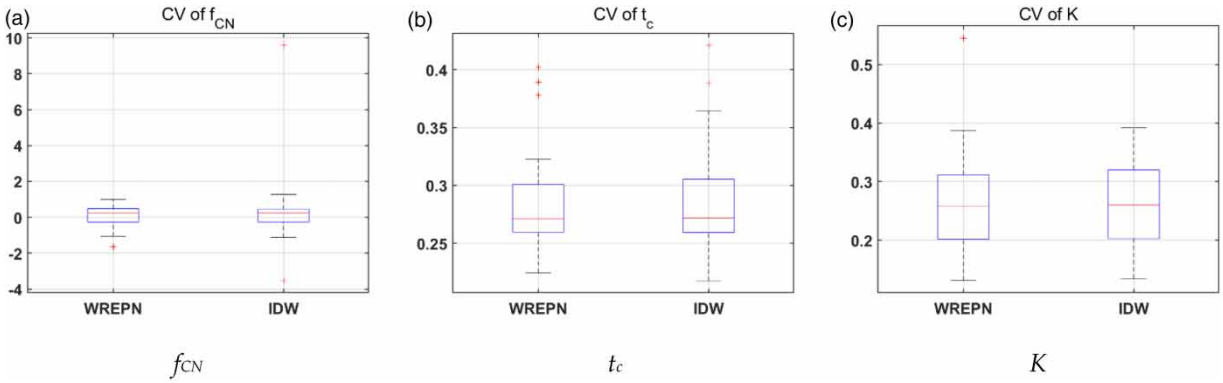

Figure 5 | Box plot of coefficient of variation for each parameter of spatial rainfall field estimation method. (a) Coefficient of variation of f_{CN}; (b) coefficient of variation of t_c; and (c) coefficient of variation of K.

showed that using the WREPN spatial rainfall field reduced the uncertainty in the f_{CN} parameter estimation for flood estimation.

Indeed, while the WREPN spatial rainfall estimation method, which considers the mountain effect in general rainfall events, showed relatively robust results, it might not be dramatically superior. However, it significantly reduced uncertainty in extreme rainfall events with observation peak rainfall exceeding 500 mm, emphasizing the importance of rainfall data in hydrological modeling. To achieve better results, further studies should explore various rainfall events, watershed conditions, and remote sensing data, aiming to generalize the findings. It is anticipated that such research will provide insights into the impact of rainfall variability and flood model parameter estimation uncertainty in mountainous regions.

This study reaffirmed the significant influence of rainfall on flood estimation and highlighted the need for continuous and related research to better understand the high variability of rainfall and its implications in flood estimation in mountainous areas.

ACKNOWLEDGEMENT

This work was supported by the National Research Foundation of Korea (NRF) grant funded by the Korea government (MSIT) (No. NRF-2022R1A2B5B01001750).

DATA AVAILABILITY STATEMENT

All relevant data are included in the paper or its Supplementary Information.

CONFLICT OF INTEREST

The authors declare there is no conflict.

REFERENCES

Abbate, A., Papini, M. & Longoni, L. 2022 Orographic precipitation extremes: An application of LUME (Linear Upslope Model Ex-tension) over the Alps and Apennines in Italy. *Water* **14**, 2218. https://doi.org/10.3390/w14142218.

Adib, A., Lotfirad, M. & Haghighi, A. 2019 Using uncertainty and sensitivity analysis for finding the best rainfall-runoff model in mountainous watersheds (Case study: The Navrood watershed in Iran). *Journal of Mountain Science* **16** (3), 529–541. https://doi.org/10.1007/s11629-018-5010-6.

Arnaud, P., Bouvier, C., Cisneros, L. & Dominguez, R. 2002 Influence of rainfall spatial variability on flood prediction. *Journal of Hydrology* **260** (1–4), 216–230. https://doi.org/10.1016/S0022-1694(01)00611-4.

Auliagisni, W., Wilkinson, S. & Elkharboutly, M. 2022 Learning from floods – How a community develops future resilience. *Water* **14**, 3238. https://doi.org/10.3390/w14203238.

Barry, R. 1992 *Mountain Weather and Climate*. Routledge, London.

Cho, Y., Engel, B. A. & Merwade, V. M. 2018 A spatially distributed Clark's unit hydrograph based hybrid hydrologic model (Distributed-Clark). *Hydrological Sciences Journal* **63** (10), 1519–1539. https://doi.org/10.1080/02626667.2018.1516042.

Clark, C. O. 1945 Storage and the unit hydrograph. *Transactions of the American Society of Civil Engineers* **110** (1), 1419–1446. https://doi.org/10.1061/TACEAT.0005800.

Cui, P., Zhou, G. G., Zhu, X. H. & Zhang, J. Q. 2013 Scale amplification of natural debris flows caused by cascading landslide dam failures. *Geomorphology* **182**, 173–189. https://doi.org/10.1016/j.geomorph.2012.11.009.

Emmanuel, I., Andrieu, H., Leblois, E., Janey, N. & Payrastre, O. 2015 Influence of rainfall spatial variability on rainfall–runoff modelling: Benefit of a simulation approach? *Journal of Hydrology* **531**, 337–348. https://doi.org/10.1016/j.jhydrol.2015.04.058.

Feldman, A. D. 2000 *HEC-HMS technical reference manual*. US Army corps of engineers R&D Woek Unit. Report, 148 p.

Furcolo, P., Pelosi, A. & Rossi, F. 2016 Statistical identification of orographic effects in the regional analysis of extreme rainfall. *Hydrological Processes* **30** (9), 1342–1353. https://doi.org/10.1002/hyp.10719.

Gabellani, S., Boni, G., Ferraris, L., Von Hardenberg, J. & Provenzale, A. 2007 Propagation of uncertainty from rainfall to runoff: A case study with a stochastic rainfall generator. *Advances in Water Resources* **30** (10), 2061–2071. https://doi.org/10.1016/j.advwatres.2006.11.015.

Gebregiorgis, A. S. & Hossain, F. 2012 Understanding the dependence of satellite rainfall uncertainty on topography and climate for hydrologic model simulation. *IEEE Transactions on Geoscience and Remote Sensing* **51** (1), 704–718. doi:10.1109/TGRS.2012.2196282.

Goovaerts, P. 2000 Geostatistical approaches for incorporating elevation into the spatial interpolation of rainfall. *Journal of Hydrology* **228** (1–2), 113–129. https://doi.org/10.1016/S0022-1694(00)00144-X.

Gottardi, F., Obled, C., Gailhard, J. & Paquet, E. 2012 Statistical reanalysis of precipitation fields based on ground network data and weather patterns: Application over French mountains. *Journal of Hydrology* **432**, 154–167. https://doi.org/10.1016/j.jhydrol.2012.02.014.

Hailemariam, S. F. & Alfredsen, K. 2023 Quantitative flood risk assessment in Drammenselva River, Norway. *Water* **15** (5), 920. https://doi.org/10.3390/w15050920.

Hastings, W. K. 1970 Monte Carlo sampling methods using Markov chains and their applications. *Biometrika* **57** (1), 97–109. https://doi.org/10.1093/biomet/57.1.97.

Houze Jr., R. A. 2012 Orographic effects on precipitating clouds. *Reviews of Geophysics* **50**, 1. https://doi.org/10.1029/2011RG000365.

Hu, K. H., Ge, Y. G., Cui, P., Guo, X. J. & Yang, W. 2010 Preliminary analysis of extra-large-scale debris flow disaster in Zhouqu County of Gansu Province. *Journal of Mountain Science* **28** (5), 628–634.

Hussain, Y., Satgé, F., Hussain, M. B., Martinez-Carvajal, H., Bonnet, M. P., Cárdenas-Soto, M., Roig, H. L. & Akhter, G. 2018 Performance of CMORPH, TMPA, and PERSIANN rainfall datasets over plain, mountainous, and glacial regions of Pakistan. *Theoretical and Applied Climatology* **131**, 1119–1132. https://doi.org/10.1007/s00704-016-2027-z.

Joo, J., Lee, J., Kim, J. H., Jun, H. & Jo, D. 2013 Inter-event time definition setting procedure for urban drainage systems. *Water* **6** (1), 45–58. https://doi.org/10.3390/w6010045.

Kim, S. & Han, S. 2010 Urban stormwater capture curve using three-parameter mixed exponential probability density function and NRCS runoff curve number method. *Water Environment Research* **82** (1), 43–50.

Kirsta, Y. B. & Troshkova, I. A. 2023 High-performance forecasting of spring flood in mountain river basins with complex landscape structure. *Water* **15** (6), 1080. https://doi.org/10.3390/w15061080.

Klijn, F., Lang, M. & Bakonyi, P. 2022 Integrated flood risk management: Novel approaches for an uncertain future. *Water Security* **17**, 100125. https://doi.org/10.1016/j.wasec.2022.100125.

Krajewski, W. F., Ciach, G. J., McCollum, J. R. & Bacotiu, C. 2000 Initial validation of the global precipitation climatology project monthly rainfall over the United States. *Journal of Applied Meteorology* **39** (7), 1071–1086. https://doi.org/10.1175/1520-0450(2000)039 < 1071:IVOTGP > 2.0.CO;2.

Kundzewicz, Z. W., Su, B., Wang, Y., Wang, G., Wang, G., Huang, J. & Jiang, T. 2019 Flood risk in a range of spatial perspectives–from global to local scales. *Natural Hazards and Earth System Sciences* **19** (7), 1319–1328. https://doi.org/10.5194/nhess-19-1319-2019.

Lee, J. S. & Choi, H. I. 2018 Comparison of flood vulnerability assessments to climate change by construction frameworks for a composite indicator. *Sustainability* **10** (3), 768. https://doi.org/10.3390/su10030768.

Lee, J. & Yoo, C. 2023 Determination of Clark unit hydrograph parameters for estimating probable maximum flood. *Hydrology Research* **54** (2), 245–264. https://doi.org/10.2166/nh.2023.120.

Lee, J., Lee, O., Choi, J., Seo, J., Won, J., Jang, S. & Kim, S. 2023 Estimation of real-time rainfall fields reflecting the mountain effect of rainfall explained by the WRF rainfall fields. *Water* **15** (9), 1794. https://doi.org/10.3390/w15091794.

Liu, X., Xia, C., Tang, Y., Tu, J. & Wang, H. 2021 Parameter optimization and uncertainty assessment for rainfall frequency modeling using an adaptive Metropolis–Hastings algorithm. *Water Science and Technology* **83** (5), 1085–1102.

Lloyd, C. D. 2005 Assessing the effect of integrating elevation data into the estimation of monthly precipitation in Great Britain. *Journal of Hydrology* **308** (1–4), 128–150. https://doi.org/10.1016/j.jhydrol.2004.10.026.

Lobligeois, F., Andréassian, V., Perrin, C., Tabary, P. & Loumagne, C. 2014 When does higher spatial resolution rainfall information improve streamflow simulation? An evaluation using 3620 flood events. *Hydrology and Earth System Sciences* **18** (2), 575–594. https://doi.org/10.5194/hess-18-575-2014.

Mie Sein, Z. M., Ullah, I., Saleem, F., Zhi, X., Syed, S. & & Azam, K. 2021 Interdecadal variability in Myanmar rainfall in the monsoon season (May–October) using eigen methods. *Water* **13** (5), 729. https://doi.org/10.3390/w13050729.

Moreno, H. A., Vivoni, E. R. & Gochis, D. J. 2014 Addressing uncertainty in reflectivity-rainfall relations in mountain watersheds during summer convection. *Hydrological Processes* **28** (3), 688–704. https://doi.org/10.1002/hyp.9600.

Nikolopoulos, E. I., Crema, S., Marchi, L., Marra, F., Guzzetti, F. & Borga, M. 2014 Impact of uncertainty in rainfall estimation on the identification of rainfall thresholds for debris flow occurrence. *Geomorphology* **221**, 286–297. https://doi.org/10.1016/j.geomorph.2014.06.015.

Obled, C., Wendling, J. & Beven, K. 1994 The sensitivity of hydrological models to spatial rainfall patterns: An evaluation using observed data. *Journal of Hydrology* **159** (1–4), 305–333. https://doi.org/10.1016/0022-1694(94)90263-1.

O'Callaghan, J. F. & Mark, D. M. 1984 The extraction of drainage networks from digital elevation data. *Computer Vision, Graphics, and Image Processing* **28** (3), 323–344.

Paudel, M., Nelson, E. J. & Scharffenberg, W. 2009 Comparison of lumped and quasi-distributed Clark runoff models using the SCS curve number equation. *Journal of Hydrologic Engineering* **14** (10), 1098–1106. https://doi.org/10.1061/(ASCE)HE.1943-5584.0000100.

Piman, T. & Babel, M. S. 2013 Prediction of rainfall-runoff in an ungauged basin: Case study in the mountainous region of Northern Thailand. *Journal of Hydrologic Engineering* **18** (2), 285–296. https://doi.org/10.1061/(ASCE)HE.1943-5584.00005.

Ragettli, S., Tong, X., Zhang, G., Wang, H., Zhang, P. & Stähli, M. 2021 Climate change impacts on summer flood frequencies in two mountainous catchments in China and Switzerland. *Hydrology Research* **52** (1), 4–25. https://doi.org/10.2166/nh.2019.118.

Ryu, Y., Moon, H., Kim, J., Kim, T. J., Boo, K. O., Guan, B., Kamae, Y., Mei, W., Park, C., Son, S. W. & Byun, Y. H. 2021 A multi-inventory ensemble analysis of the effects of atmospheric rivers on precipitation and streamflow in the Namgang-Dam Basin in Korea. *Water Resources Research* **57** (8), e2021WR030058. https://doi.org/10.1029/2021WR030058.

Sangati, M. & Borga, M. 2009 Influence of rainfall spatial resolution on flash flood modelling. *Natural Hazards and Earth System Sciences* **9** (2), 575–584. https://doi.org/10.5194/nhess-9-575-2009.

Saouabe, T., El Khalki, E. M., Saidi, M. E. M., Najmi, A., Hadri, A., Rachidi, S., Jadoud, M. & Tramblay, Y. 2020 Evaluation of the GPM-IMERG precipitation product for flood modeling in a semi-arid mountainous basin in Morocco. *Water* **12** (9), 2516. https://doi.org/10.3390/w12092516.

Singh, V. P. 1997 Effect of spatial and temporal variability in rainfall and watershed characteristics on stream flow hydrograph. *Hydrological Processes* **11** (12), 1649–1669. https://doi.org/10.1002/(SICI)1099-1085(19971015)11:12 < 1649::AID-HYP495 > 3.0.CO;2-1.

Skaugen, T., Peerebom, I. O. & Nilsson, A. 2015 Use of a parsimonious rainfall–run-off model for predicting hydrological response in ungauged basins. *Hydrological Processes* **29** (8), 1999–2013. https://doi.org/10.1002/hyp.10315.

Stoffel, M., Wyżga, B. & Marston, R. A. 2016 Floods in mountain environments: A synthesis. *Geomorphology* **272**, 1–9. https://doi.org/10.1016/j.geomorph.2016.07.008.

Tedela, N. H., McCutcheon, S. C., Rasmussen, T. C., Hawkins, R. H., Swank, W. T., Campbell, J. L., Adams, M. B., Jackson, C. R. & Tollner, E. W. 2012 Runoff curve numbers for 10 small forested watersheds in the mountains of the eastern United States. *Journal of Hydrologic Engineering* **17** (11), 1188–1198. https://doi.org/10.1061/(ASCE)HE.1943-5584.00004.

Tobin, C., Nicotina, L., Parlange, M. B., Berne, A. & Rinaldo, A. 2011 Improved interpolation of meteorological forcings for hydrologic applications in a Swiss Alpine region. *Journal of Hydrology* **401** (1–2), 77–89. https://doi.org/10.1016/j.jhydrol.2011.02.010.

USDA, S. 1986 *Urban Hydrology for Small Watersheds TR-55. Technical Release*. United States Department for Agriculture Soil Conservation Service, Washington, DC.

Verma, S., Verma, R. K., Mishra, S. K., Singh, A. & Jayaraj, G. K. 2017 A revisit of NRCS-CN inspired models coupled with RS and GIS for runoff estimation. *Hydrological Sciences Journal* **62** (12), 1891–1930. https://doi.org/10.1080/02626667.2017.1334166.

Vieux, B. E., Park, J. H. & Kang, B. 2009 Distributed hydrologic prediction: Sensitivity to accuracy of initial soil moisture conditions and radar rainfall input. *Journal of Hydrologic Engineering* **14** (7), 671–689. https://doi.org/10.1061/(ASCE)HE.1943-5584.000003.

Wu, Y., Xue, L., Liu, Y. & Ren, L. 2019 Uncertainty assessment of extreme flood estimation in the Dongting Lake basin, China. *Hydrology Research* **50** (4), 1162–1176. https://doi.org/10.2166/nh.2019.088.

Xiaojun, G., Peng, C., Xingchang, C., Yong, L., Ju, Z. & Yuqing, S. 2021 Spatial uncertainty of rainfall and its impact on hydrological hazard forecasting in a small semiarid mountainous watershed. *Journal of Hydrology* **595**, 126049. https://doi.org/10.1016/j.jhydrol.2021.126049.

Yoon, Y. N., Kim, J. H., Yoo, C. S. & Kim, S. D. 2002 A runoff parameter estimation using spatially distributed rainfall and an analysis of the effect of rainfall errors on runoff computation. *Journal of Korea Water Resources Association* **35** (1), 1–12.

Younger, P. M., Freer, J. E. & Beven, K. J. 2009 Detecting the effects of spatial variability of rainfall on hydrological modelling within an uncertainty analysis framework. *Hydrological Processes* **23** (14), 1988–2003. https://doi.org/10.1002/hyp.7341.

Zhang, J. & Han, D. 2017 Assessment of rainfall spatial variability and its influence on runoff modelling: A case study in the Brue catchment, UK. *Hydrological Processes* **31** (16), 2972–2981. https://doi.org/10.1002/hyp.11250.

First received 1 September 2023; accepted in revised form 15 January 2024. Available online 31 January 2024